**Proceedings of the ASME 2014 33rd International Conference on Ocean, Offshore and Arctic Engineering**
**OMAE2014**
**June 8-13, 2014, San Francisco, California, USA**

**OMAE2014-23358**

# THEORY AND EXPERIMENTS OF A FREE-RUNNING FISHING VESSEL IN STERN SEA

**Maxime Thys**
Centre for Ships and Ocean Structures,
Department of Marine Technology,
Norwegian University of Science and Technology
Trondheim, Norway

**Odd Magnus Faltinsen**
Centre for Ships and Ocean Structures,
Department of Marine Technology,
Norwegian University of Science and Technology
Trondheim, Norway

## ABSTRACT

Hydrodynamic aspects of a modern fishing vessel during manoeuvring in a seaway was studied theoretically and experimentally. The focus was on small frequencies of encounter, corresponding to following and stern quartering seas, where fishing vessels are susceptible to capsize. The numerical model was based on de Kat and Paulling [1]. The model combined a 6 degrees of freedom (DOF) blended seakeeping model with a 4 DOF non-linear manoeuvring model. The 3D non-linear Froude-Krylov and restoring loads were computed by pressure integration up to the incident free surface. The added mass, damping and wave diffraction loads were obtained by generalizing the STF (Salvesen *et al.* [2]) strip theory to partly include 3D flow effects by means of WAMIT.

The simulated wave-induced surge forces over-estimated the experimentally measured forces by up to 50%. Excessive wave-induced surge forces led to predictions of broaching and surf riding, which did not occur in the experiments. Use of experimentally determined wave-induced surge forces gave good agreement between simulations and experiments.

## 1 INTRODUCTION

Stability against capsizing of ships in heavy seas is important when designing small ships. The most vulnerable headings in heavy seas are following and quartering seas with small frequency of encounter, where broaching can occur.

Different methods are available to study ship manoeuvring in a seaway; such as full-scale experiments, model scale experiments, and simulations. The current state of the art to simulate the ship behaviour in a seaway is by use of a simplified mathematical model. Other methods such as CFD require a significant amount of computational time compared to a simplified mathematical model, and may still contain large uncertainties in the modelling of propagating waves[1]. Since the considered frequency of encounter is small, the two-time scale method by Skejic and Faltinsen [3] for ship manoeuvring in waves is not applicable. However, elements in the presented manoeuvring model have similarities. A difference is that the important effect of waves on ship manoeuvring in the two-time scale method is through speed- and heading-dependent mean wave loads. However, mean wave loads are generally small at low frequencies of encounter.

Different simplified mathematical models have been developed over time to study ships in following to stern quartering seas [1, 4, 5]. The mathematical models were able to simulate different ship behaviours such as surf-riding and broaching. The environmental conditions leading to these behaviours are more difficult to identify by simulations, and it is felt that there is still room for improvement.

The behaviour of a ship at small frequency of encounter is studied here by use of simulations and experiments at model scale. The simulation model is based on the current state of the art. New experiments were performed to validate the simulation model, and to study the behaviour of a ship at small frequency of encounter in stern sea.

## 2 *LADY MARIANNE*

A new model, called *Lady Marianne*, was constructed for the experiments, and was based on a 21 m modern fishing vessel with a large ship beam-to-length ratio. The body and lines plan of the model are shown in Fig. 1 and the main dimensions of the model are given in Tab. 1. The model has two bilge keels and a single rudder in the wake of a ducted

[1] The Final Report and Recommendations to the 26th ITTC from The Specialist Committee on Computational Fluid Dynamics

propeller. A turbulence trigger wire of 1 mm in diameter was installed at the bow.

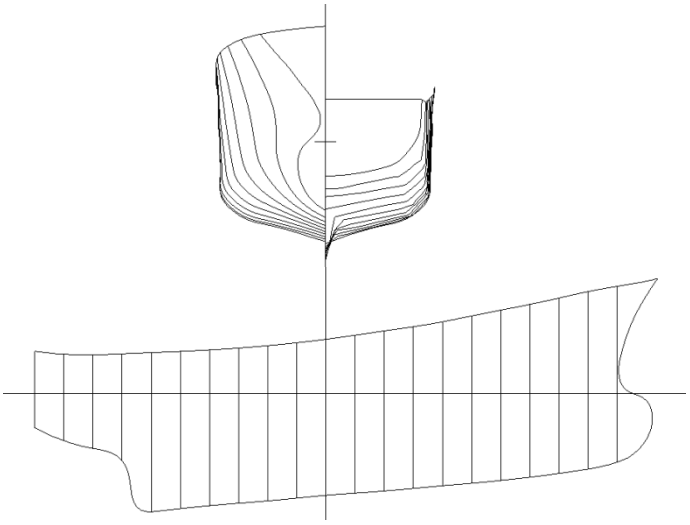

**FIGURE 1: Body and lines plan of the *Lady Marianne***

**TABLE 1: Principal particulars of the *Lady Marianne***

| Items | Model |
|---|---|
| Length between perpendiculars: $L_{pp}$ | 0.800 m |
| Length at the waterline: $L_{wl}$ | 0.850 m |
| Beam: $B$ | 0.300 m |
| Draft at centre of gravity: $D$ | 0.144 m |
| Displacement $\Delta$ | 22.5 kg |
| Block Coefficient: $C_B$ | 0.540 |
| Longitudinal centre of gravity from stern | 0.413 m |
| Metacentric height: $GM$ | 0.018 m |
| Radius of gyration in roll: $k_{xx}/B$ | 0.337 |
| Radius of gyration in pitch: $k_{yy}/L$ | 0.272 |
| Radius of gyration in yaw: $k_{zz}/L$ | 0.272 |
| Propeller diameter: $D_p$ | 0.060m |
| Propeller pitch over diameter ratio: $P/D_p$ | (see sect. 5) |
| Number of propeller blades: $n$ | 3 |
| Nozzle length | 0.030 m |
| Nozzle diameter[2] | 0.064 m |
| Maximum rudder angle: $\delta_{max}$ | 35º |
| Maximum rudder speed: $\dot{\delta}$ | 15º/s |
| Number of bilge keels | 2 |
| Length of each bilge keel | 0.270 m |
| Width of each bilge keel | 0.017 m |

For the free-running experiments, the model was equipped with a micro-controller, two batteries, an electrical motor for the propeller, a servomotor for the rudder, and a wireless transceiver. The ship position in the tank was measured by an optical positioning system. The ship was controlled by an autopilot, which used a PD controller when navigating on a straight line, with the proportional gain $k_p = 1.0$ and the derivative gain $k_d = 0.24$ s.

The experiments were repeated a sufficient number of times to determine a 95% confidence interval. The free-running experiments and the captive experiments in waves were performed in the Marine Cybernetics Laboratory at NTNU, Trondheim. The laboratory is 40 m long, 6.45 m wide, and 1.50 m deep, and has a wavemaker at one of the short ends. The captive experiments in calm water were performed in the 25 m long, 2.8 m wide, and 1.0 m deep Tank II at the Marine Technology Centre, NTNU. Both the experimental and numerical results are presented in model scale. Additional information about the ship model and the setup in the experiments is given in Thys [6].

## 3 THE SIMULATION MODEL

A modular mathematical model for simulating ship manoeuvring in a seaway in real-time at prototype scale was developed by combining a 6 degrees of freedom (DOF) seakeeping model with a 4 DOF non-linear manoeuvring model. The equations of motions are formulated in a lateral manoeuvring coordinate system, restrained in roll and in pitch.

The seakeeping part generalizes the Salvesen-Tuck-Faltinsen (STF) strip theory [2] to include partly 3D flow effects by means of WAMIT. It means that the free-surface and body-boundary conditions are the same as in the STF theory, e.g. interaction with local steady flow is neglected. Further, the free-surface condition does not correctly model the unsteady wave systems. The pressure is expressed similarly as in strip theory. Strictly speaking, the STF theory is a high-frequency theory for slender ships at moderate Froude numbers. However, it is used in engineering practise in a broader range. A generalized Haskind relation obtains the total diffraction loads on the ship in a similar way as in the STF theory. The difference from strip theory is that the 3D Laplace equation is solved by means of WAMIT. A similar formulation was used by Beck and Loken [7], Papanikolaou and Schellin [8], and McTaggart [9]. The hydrodynamic loads in the time domain due to sway, heave, roll, pitch and yaw are based on Cummins [10] formulation in terms of convolution integrals. The corresponding retardation functions were calculated by means of the frequency-domain damping coefficients. The hydrodynamic loads due to surge were based on zero-frequency added mass coefficients.

The non-linear Froude-Krylov and hydrostatic loads were obtained by properly integrating pressure on an instantaneous wetted surface defined by the ship motions and the wave elevation at the hull according to second-order Stokes waves.

The 6 DOF seakeeping model was combined with a non-linear manoeuvring model in order to simulate the ship slow-down in a turn during manoeuvres with large changes in the heading angle. The non-linear manoeuvring model was based on a combination of slender body theory and added mass theory (Söding [11]). The hull force $(F_1, F_2, F_3)$ and moment $(F_4, F_5, F_6)$ due to the manoeuvring model are

[2] The nozzle inner diameter measured at the propeller location.

$$F_1 = -A_{11}^0(0)\dot{u} + C_{tn}A_{22}^0(0)vr + A_{24}^0(0)pr + A_{26}^0(0)r^2, \quad (1)$$

$$F_2 = -A_{22}^0(0)\dot{v} - A_{24}^0(0)\dot{p} - A_{26}^0(0)\dot{r} - A_{11}^0(0)ur - a_{22}^A(0)uv - a_{24}^A(0)up - a_{22}^A(0)x_A ur, \quad (2)$$

$$F_4 = -A_{42}^0(0)\dot{v} - A_{44}^0(0)\dot{p} - A_{46}^0(0)\dot{r} - a_{42}^A(0)uv - a_{44}^A(0)up - a_{42}^A(0)x_A ur, \quad (3)$$

$$F_6 = -A_{62}^0(0)\dot{v} - A_{64}^0(0)\dot{p} - A_{66}^0(0)\dot{r} - [A_{22}^0(0) + a_{22}^A(0)x_A]uv - [A_{24}^0(0) + a_{24}^A(0)x_A]up - [A_{26}^0(0) + a_{22}^A(0)x_A^2]ur + A_{11}^0(0)uv, \quad (4)$$

where $x_A$ is the longitudinal position of the ship section where flow separation occurs. $A_{ij}^0(0)$ is the added mass in mode $i$ due to motion in mode $j$ at zero forward speed and zero frequency of encounter. Further, $a_{ij}^A(0)$ is the zero-frequency sectional added mass of the ship section where the flow separation occurs. $u$, $v$, $p$, and $r$ are ship velocities in surge and sway of COG and angular roll and yaw velocities, respectively. The subscripts 1, 2, 4, and 6 correspond to surge, sway, roll, and yaw, respectively.

When combining the seakeeping model and the manoeuvring model, special care is needed to avoid duplicating forces in the formulation and to account for the differences in the manoeuvring and seakeeping coordinate systems.

Separate modules based on a mixture of empiricism, simplified theoretical methods, and experimental results modelled the resistance, propulsion, rudder, and viscous loads.

## 4 MODULES OF THE SIMULATION MODEL

The calm water resistance $R_t$ of *Lady Marianne* was obtained by towing the hull in Tank II. The experimental results with a 95% confidence interval are shown in Fig. 2. Exponential regression analysis of the experimental results gave for the ship resistance

$$R_t = 7.074 \cdot 10^{-2} e^{3.846u} - 7.074 \cdot 10^{-2}, \quad (5)$$

Where $R_t$ is in N and $u$ is the calm water forward speed in m/s. The formula applies only to our model scale. The comparison between the experimental results, the resistance based on the Digernes [12] formulation and the regression formula is shown in Fig. 2.

The 3D boundary element program developed by Ommani [13] was used to calculate the calm-water wave resistance in order to ensure that there are no "humps and hollows" in the speed-dependent resistance. Since no "humps and hollows" were found, resistance formula (5) was used for all speeds. When Eq. (5) is used in the simulation model, $u$ includes unsteady effects.

The propulsion forces in the simulation model were based on the Wageningen ducted propeller series (Oosterveld [14]). The verification of the propulsion module was performed by use of the calm water straight line manoeuvres, as explained in section 5.

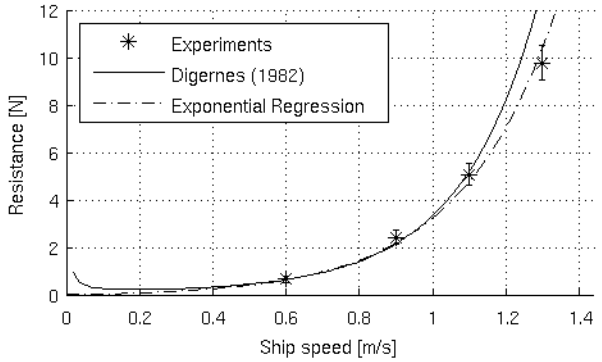


**FIGURE 2: Calm water resistance based on experiments versus the empirical formula by Digernes [12] and the exponential regression formula implemented in the simulation model.**

The hull-propeller interaction was modelled by use of the thrust deduction coefficient $t$ and the wake factor $w$.

A constant thrust deduction coefficient $t = 0.208$ was used, based on Weingart [15]. The wake factor as a function of forward speed was measured by use of a Pitot tube at the propeller plane during towing of the bare hull.

The experimentally determined wake factor is shown in Fig. 3 for different forward speeds. The wake factor varies with the forward speed, where the decrease is believed to be mainly due to the frictional wake for lower Froude numbers and the increase due to the wave wake for the higher speeds. The figure also shows predictions based on the forward-speed independent empirical formula by Taylor [16], which agrees poorly with the experiments.

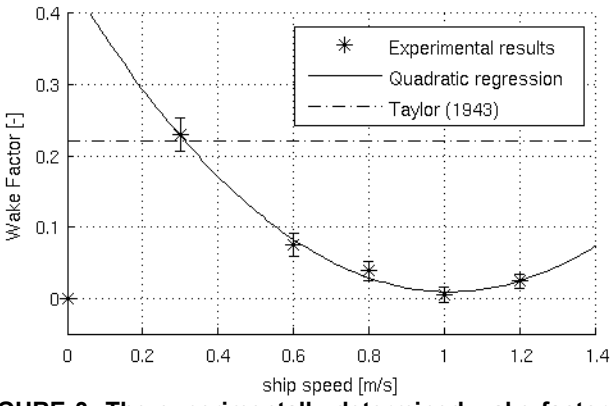


**FIGURE 3: The experimentally determined wake factor and the regression formula used in the simulation model.**

The wake factor was expressed in the simulation model based on a quadratic regression of the experimental results, as

$$w = 0.430u^2 - 0.872u + 0.451, \quad (6)$$

where $u$ is the ship forward in m/s. The formula applies only to our model scale.

The rudder is modelled in the simulation tool as a single rudder in the wake of a propeller. The computed rudder forces account for the flow influence of the propeller on the rudder in a similar way as presented by Ankudinov *et al.* [17]. Since an accurate estimate of the rudder forces is crucial for accurate manoeuvring predictions, experiments were performed to measure the rudder forces.

In the experiments, the ship model was connected to the carriage and towed with different forward speeds and with different rudder angles $\delta$, while the propeller was rotating with a constant RPM. Force transducers were used between the carriage and the model. The measured side forces were considered as due to the rudder only. Measuring the rudder forces on the rudder shaft directly was impossible due to the small size of the model.

The rudder lift coefficient was defined as $C_L = 2F_2^{rud}/(\rho A_r V_r^2)$ where $F_2^{rud}$ is the side force delivered by the rudder, $A_r$ is the rudder projected area, and $V_r$ is the velocity of the flow over the rudder. The experimentally determined lift coefficient is compared to the formulation of Bertram [18] and Inoue *et al.* [19] in Fig. 4. The two formulas over-predict the rudder lift coefficient, and thus the rudder force by more than 25% for $\delta \geq 15^o$. There is an over-prediction of 92% for the lift coefficient proposed by Bertram at $\delta = 35^o$.

Fig. 4 also presents a quadratic regression formula for the rudder lift coefficient based on the experiments. The formula is

$$C_L = -7.749 \cdot 10^{-4}\alpha_d^2 + 5.691 \cdot 10^{-2}\alpha_d, \qquad (7)$$

where $\alpha_d$ is the angle between the rudder and the inflow to the rudder, in degrees. Eq. (7) was used in the simulations with the *Lady Marianne*.

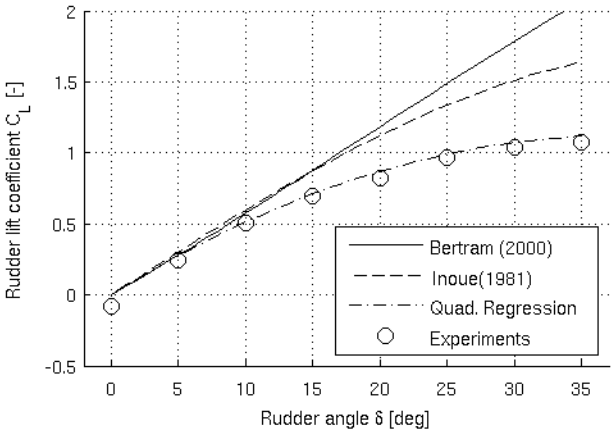


**FIGURE 4: The experimentally determined rudder lift coefficient as a function of rudder angle versus experimentally based quadratic regression formula and formulas by Bertram [18] and Inoue *et al.* [19].**

The non-linear transverse viscous force $F_2^{cf}$ and yaw moment $F_6^{cf}$ due to sway and yaw velocities are computed by the cross-flow principle (Faltinsen [20]). An artificial constant sectional drag coefficient $C_D$ was used and determined by captive experiments, where the bare hull of the *Lady Marianne* was towed at different forward speeds $U$ and with different drift angles $\beta$. The measured side force $F_2$ was compared to the simulated side force, which consists of a hull-lift term and a viscous cross-flow term and is expressed as

$$F_2 = -a_{22}^A(0)uv + F_2^{cf}, \qquad (8)$$

where $a_{22}^A(0)$ is the zero-frequency 2D sway added mass at the longitudinal position where flow separation occurs. The latter position (0.267 m aft of the ship centre of gravity) was indirectly found from the experimental results at very small drift angles ($|\beta| \leq 5^o$), when the side force due to the viscous cross-flow is negligible and the side force is mainly due to hull lift.

When using $C_D = 1.3$, the numerical predictions agreed well with the experiments even though the cross-flow principle is questionable at small drift angles ($|\beta| < 20^o$). The measured side force and the simulated side force are shown in Fig. 5, for different drift angles $\beta$ and for different forward speeds $U$ defined in the figure.

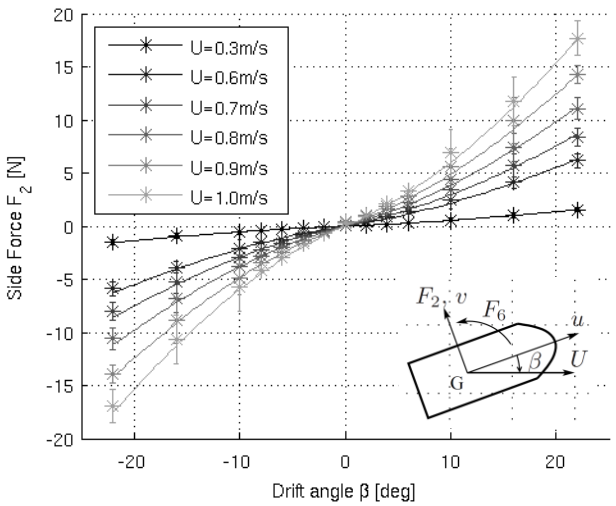


**FIGURE 5: Experimental (*) and simulated (-) side force $F_2$ on the *Lady Marianne* moving forward at different forward speeds $U$ and with different drift angles $\beta$.**

The applied viscous cross-flow roll moment is (Söding [21])

$$F_4^{cf} = (KG - 0.65D)F_2^{cf}, \qquad (9)$$

where $D$ is the ship draft, and $KG$ is the vertical distance between the ship keel and the centre of gravity.

The viscous roll damping used in the simulation program was expressed as linear and quadratic damping terms that was determined from roll decay experiments at zero forward speed [6]. The fact that the viscous roll damping is forward-speed dependent is an error source.

## 5 CALM WATER MANOEUVRES

Calm water experiments were performed with the *Lady Marianne* to verify the propulsion module, to determine the reduction coefficient $C_{tn}$ in the surge equation of motion (see Eq. (1)), and to validate the simulation model in calm water.

The calm-water straight-line manoeuvres were used to verify the correct modelling of the propulsion forces. In the manoeuvre, the model starts from rest, and navigates on a straight line by use of a PD-autopilot with different propeller RPMs.

The simulated calm water forward speeds over-predicted the experimentally obtained forward speeds, probably due to scale effects and geometrical differences between the ducted propeller used in the Wageningen ducted propeller series and the one on the *Lady Marianne*. By changing the propeller pitch over diameter ratio $P/D_p$ in the simulation model, a good agreement was obtained between the simulated and the experimental calm water forward speed on a straight line. The geometrically measured pitch over diameter ratio was 1.23, and a ratio of 0.78 was used in the simulation model.

The simulated and experimental calm water forward speeds are shown in Fig. 6 for different propeller RPM. Based on the calm water straight line manoeuvres, the modelling of the propulsion and resistance forces was judged satisfactory.

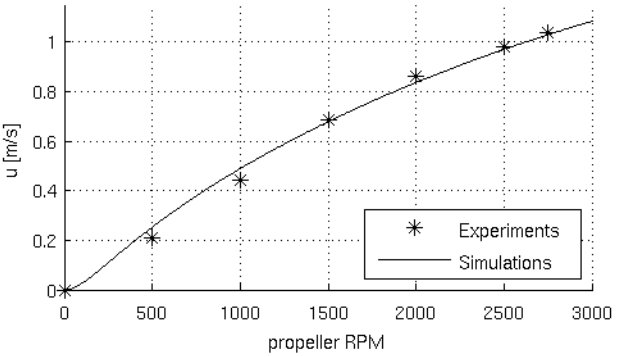


**FIGURE 6: Experimental and simulated calm water forward speed *u* of the *Lady Marianne* on a straight line for different propeller RPM.**

By comparing the simulated and experimental path of the *Lady Marianne* during the calm water turning circle manoeuvres, the reduction coefficient $C_{tn}$ (see Eq. (1)) was selected as 0.6.

Six different turning circle manoeuvres were realized, with varying propeller RPM (1200, 2000, 2750) and rudder angle ($-25°$,$-35°$). The characteristic parameters of the turning circle manoeuvres (advance, transfer, tactical diameter and steady diameter) were compared between experiments and simulations [6] and the agreement was found satisfactory. The agreement between the simulated and the experimental path of the *Lady Marianne* during one of the turning circle manoeuvres is shown in Fig. 7 The ship starts from rest, moves on a straight line for 15 s, and starts then the turning circle manoeuvre with a rudder angle $\delta$ of $-25°$. The propeller RPM is 2750 during the manoeuvre.

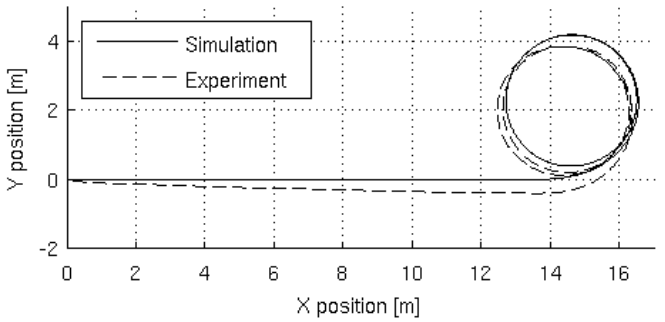


**FIGURE 7: Experimental and simulated path of the *Lady Marianne* during a turning circle manoeuvre in calm water (RPM=2750 and $\delta = -25°$).**

The sensitivity of the simulation model to the wake factor $w$, the thrust deduction coefficient $t$, the reduction factor $C_{tn}$, the position of the flow separation section (for the hull-lift forces), the rudder lift coefficient $C_L$, and the cross-flow drag coefficient $C_D$ was studied based on the calm water turning circle manoeuvre. It was found that that the wake factor $w$, the thrust deduction coefficient $t$, and the reduction factor $C_{tn}$ have a small influence on the simulated ship behaviour. The position of the flow separation section can have a large influence on the ship behaviour when the section is positioned in an area where a small change in position induces a large change in the sectional sway added mass. The ship behaviour is sensitive to the rudder lift coefficient $C_L$ and the cross-flow drag coefficient $C_D$. Use of an inappropriate rudder lift coefficient can lead to predictions of e. g. 30% smaller turning circle diameters.

Zigzag manoeuvres with different propeller RPM and rudder angles $\delta$ were also performed and compared to simulations [6].

Turning circle manoeuvres are adequate to study the turning capability of the ship, while zigzag manoeuvres are adequate to study the course keeping ability of the ship. Since the simulated and experimental characteristics of the turning circle and the zigzag manoeuvre showed a satisfactory agreement, we anticipated that the simulation model is applicable for a wide variety of manoeuvres in calm water.

## 6 WAVE-INDUCED SURGE FORCES IN FOLLOWING SEAS

The wave-induced surge forces in following regular waves were examined by simulations and towing experiments of *Lady Marianne* rigidly connected to the carriage at a forward speed of 1 m/s ($Fn = 0.346$). The waves had a wavelength over ship length ratio $\lambda/L_{wl}$ of 1.0, 1.5, 2.0, or 2.5, and a wave height over wav-length ratio of $H/\lambda = 1/25$. A force sensor was used at the connection point between the carriage and the ship model to measure the forces in surge.

The maximum and minimum experimental surge forces are given in Fig. 8 for different wave length over ship length ratios

$\lambda/L_{wl}$ and compared with theoretical results consisting of ship resistance $R_t$, the Froude-Krylov force in surge $F_1^{FK}$, and the diffraction force in surge $F_1^{\text{Diff}}$. Using only the ship resistance and the Froude-Krylov force gives large over-predictions of the extremes of the surge force. The diffraction force reduces the extremes of the surge force, but the simulations still over-predict the extremes, as seen in Fig. 8.

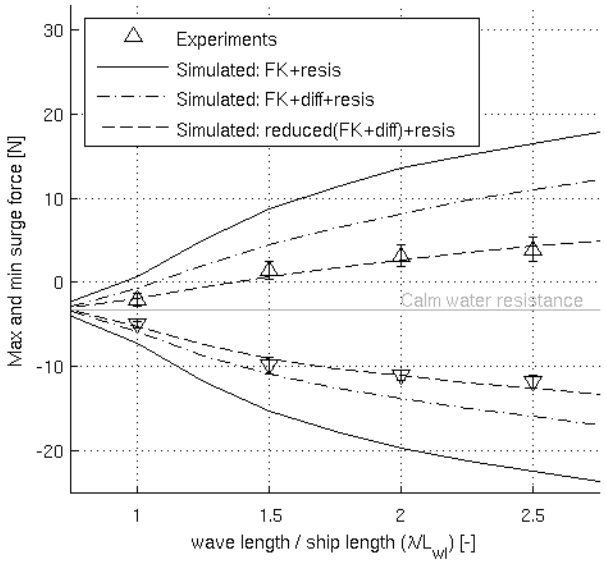


**FIGURE 8: Experimental and simulated maximum and minimum surge force on the *Lady Marianne* in following seas $\left(\frac{H}{\lambda}=\frac{1}{25}\right)$ at $Fn = 0.346$.**

Different elements in the simulation model were studied to try to reduce the differences between the simulated and the experimental surge force, such as use of higher order than second-order wave theory, the formulation of the free-surface condition for the computation of the diffraction forces, and the influence of the regular incoming waves on the ship resistance [6]. However, none of these elements could explain the significant differences between the simulated and the experimental surge force. Since the ship has relatively small length-to-beam ratio, the theoretically neglected interaction between the local steady and unsteady flow may contribute to the large differences between the experimental and numerical wave-induced surge forces.

Reduction coefficients were used for the surge excitation forces $F_1^{\text{excit}}$ in the simulations to obtain a good representation of the surge forces,

$$F_1^{\text{excit}} = \begin{cases} 0.75\left(F_1^{FK} + F_1^{\text{Diff}}\right) & \text{when } F_1^{FK} + F_1^{\text{Diff}} \le 0, \\ 0.50\left(F_1^{FK} + F_1^{\text{Diff}}\right) & \text{when } F_1^{FK} + F_1^{\text{Diff}} > 0. \end{cases} \quad (10)$$

The forces in surge, with the reduction coefficients, are shown in Fig. 8

Note that the reduction coefficients are only valid for the *Lady Marianne* navigating with a forward speed of 1 m/s in following regular waves with a wave height over wave length ratio of $H/\lambda = 1/25$.

## 7 FREE RUNNING MANOEUVRES AT SMALL FREQUENYC OF ENCOUNTER

Manoeuvring of *Lady Marianne* in a seaway (at small frequency of encounter) was studied through three different manoeuvres: a straight line manoeuvre, a turning circle manoeuvre, and a zigzag manoeuvre.

In the straight line manoeuvre in following seas, the ship was controlled by the autopilot to navigate with a heading angle $\beta = 0°$. The desired heading angle $\beta$ and the ship yaw angle $\psi$ are defined in Fig. 9.

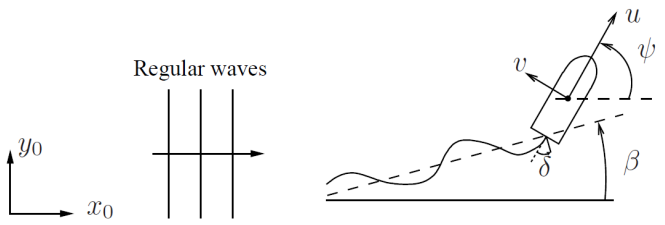


**FIGURE 9: Straight line manoeuvre in stern seas. $\beta$ is the desired heading angle, $\psi$ is the yaw angle, $\delta$ the rudder angle, and $u$ and $v$ are the longitudinal and transverse ship speeds.**

The manoeuvre is used to study the balance between ship resistance, ship propulsion, and wave-induced surge forces. The balance between these forces also leads to the discussion about surf-riding and the related broaching in stern seas. The different environmental conditions used in the experiments are summarised in Tab. 2. The propeller rotated with 2750 RPM corresponding to a ship speed $u = 1.04$ m/s ($Fn = u/\sqrt{gL_{wl}} = 0.360$) in calm water.

**TABLE 2: Wave and operational conditions for the straight line manoeuvres of *Lady Marianne* in stern seas. $H$ = wave height, $\lambda$ =wavelength, $\beta$=desired ship heading angle, $L_{wl}$= ship length at the waterline.**

| H/λ | RPM | β | λ/L$_{wl}$ |
|---|---|---|---|
| 1/25 | 2750 | 0° | 1.25, 1.50, 2.00 |
| 1/10 | 2750 | 0° | 0.75, 1.00, 1.25, 1.50, 1.75, 2.00 |
| 1/8 | 2750 | 0° | 1.25, 1.50, 2.00 |

The procedure used in the experiments was as follows:
(1) The ship is free, at rest, and positioned with $\psi = 0°$ at approximately 2 m from the wavemaker and at approximately 3 m from the side of the tank.
(2) The wavemaker is activated at $t = -aT$, where $T$ is the wave period and $a = 30, 25, 20, 15, 15, 10$ for $\lambda/L_{wl} = 0.75, 1.00, 1.25, 1.50, 1.75, 2.00$, respectively. The ship is then drifting with a natural tendency to stay with $\psi = 0°$.
(3) At $t = 0$, the propeller and the rudder autopilot are turned on, where the time $aT$ is needed to avoid the ship to pass the wave front during the manoeuvre. The propeller is controlled to rotate at the desired RPM, and the autopilot controls the rudder to navigate on a straight line with the desired heading angle $\beta$.

The different steps in the procedure are illustrated in Fig. 10. The same procedure was used in the experiments and in the

simulations. Note that the simulations in following seas were actually performed with $\beta = 1°$ to trigger possible instabilities in the coursekeeping behaviour of the ship.

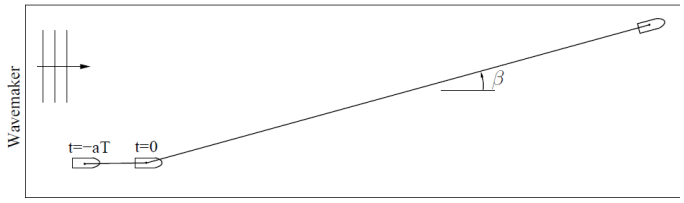


**FIGURE 10: The different steps during the straight line manoeuvre in stern seas with a desired heading angle $\beta$. The wavemaker is activated at $t = -aT$, where $T$ is the wave period and $a$ is dependent on the wave length. At $t = 0$ s, the propeller and the autopilot are activated.**

Two characteristic values were used to compare the simulations with the experiments:

- the maximum forward ship speed $u_{\max}$ encountered during a run,
- the maximum absolute heading angle $|\psi|_{\max}$ encountered when the ship is driven by the propeller and on course.

The maximum forward speed and the maximum absolute heading angle, during the manoeuvres in following seas ($\beta = 0°$), for different wave steepnesses $H/\lambda$ and different ratios of wave length over ship length $\lambda/L_{wl}$ are shown in Fig. 11 and 12. In the simulations, the reduction coefficients detailed in Eq. (10) were not used.

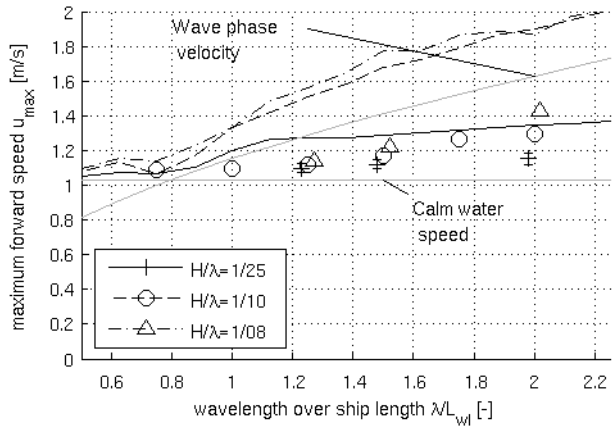


**FIGURE 11: Simulated (line) and experimental (symbol) maximum ship speed $u_{\max}$ during straight line manoeuvres in following seas ($\beta = 0°$), for different wave steepnesses $H/\lambda$ and different ratios of wave length over ship length $\lambda/L_{wl}$.**

The simulations over predicted the maximum forward speed. The ship was surf-riding in the simulations with:

- $\frac{H}{\lambda} = 1/25$ and $0.8 \leq \frac{\lambda}{L_{wl}} \leq 1.2$,
- $\frac{H}{\lambda} = 1/10$ and $\frac{\lambda}{L_{wl}} \geq 0.8$,
- $\frac{H}{\lambda} = 1/8$ and $\frac{\lambda}{L_{wl}} \geq 0.8$,

where surf-riding is defined here as the behaviour where the ship is forced by the waves to move with a constant speed equal to the wave celerity. Surf-riding with a constant forward speed was not observed in the experiments. Note that surf riding cannot be experimentally determined based on the maximum forward speed, but was determined by looking at the ship behaviour in time.

The maximum absolute yaw angles were smaller than $\pm 15°$ in the experiments, while very large maximum yaw angles are seen in the simulations.

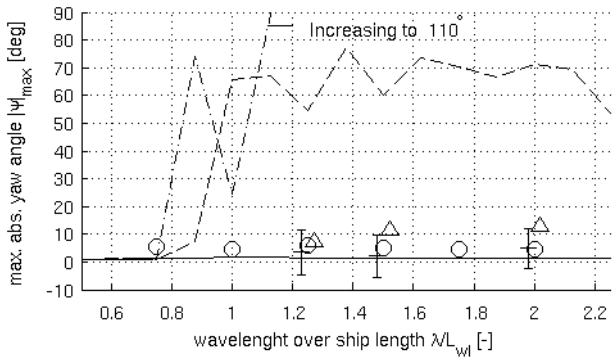


**FIGURE 12: Simulated (line) and experimental (symbol) maximum absolute yaw angle $|\psi|_{\max}$ during straight line manoeuvres in following seas ($\beta = 0°$), for different wave steepnesses $H/\lambda$ and different ratios of wavelength over ship length $\lambda/L_{wl}$. Same legend as in Fig. 11.**

Surf-riding behaviour and large yaw angles are clear indications of broaching in the simulations. Broaching was not observed in the experiments but occurred in the simulations for $H/\lambda = 1/10$ and 1/8, and for $\lambda/L_{wl} > 0.8$.

A simulation with broaching is shown in Fig. 13, where the *Lady Marianne* is navigating with a propeller RPM of 2750. The wave steepness is $H/\lambda = 1/10$, and the wavelength over ship length ratio $\lambda/L_{wl} = 1.50$. The surf-riding behaviour of the ship is seen for $6\text{ s} < t < 9\text{ s}$. A yaw motion is initiated when the ship is surf-riding, and the autopilot tries to counteract this yaw motion. Maximum rudder angle is reached at $t = 9$ s, when the ship is still off course as the rudder forces are not sufficient to stop the yaw motion.

For the simulations with the smallest wave steepness ($H/\lambda = 1/25$), the reduction coefficients for the wave excitation forces in surge (see Eq. (10)) can be used to obtain better predictions of the maximum forward speed. The simulated maximum forward speed is accurately predicted with the reduction coefficients and is shown in Fig. 14.

The reduction coefficients are only valid for the same conditions as measured in the captive experiments ($H/\lambda = 1/25$). For the larger wave steepnesses, even larger reduction coefficients are necessary to obtain a good agreement between simulated and experimental maximum forward speed.

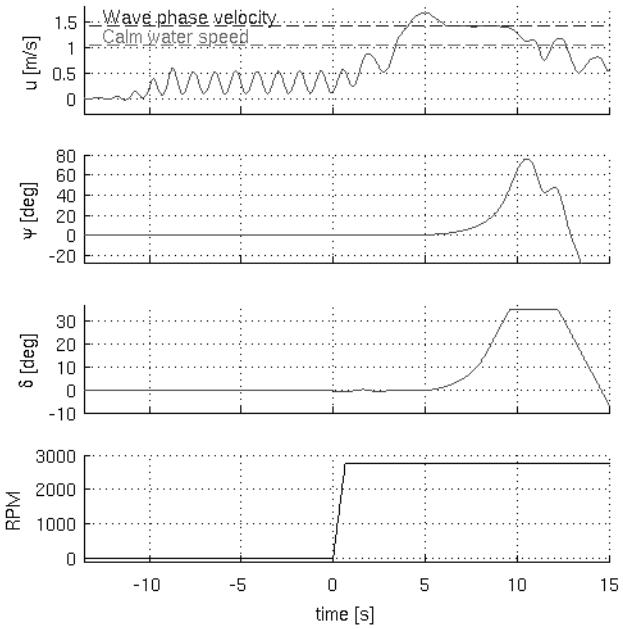


**FIGURE 13: Simulated ship forward speed $u$, yaw angle $\psi$, rudder angle $\delta$, and propeller RPM during a straight line manoeuvres in regular following seas ($\beta = 0°$), with a wave steepness $H/\lambda = 1/10$ and a ratio of wave length over ship length $\frac{\lambda}{L_{wl}} = 1.50$. Broaching occurred at $t > 6$ s.**

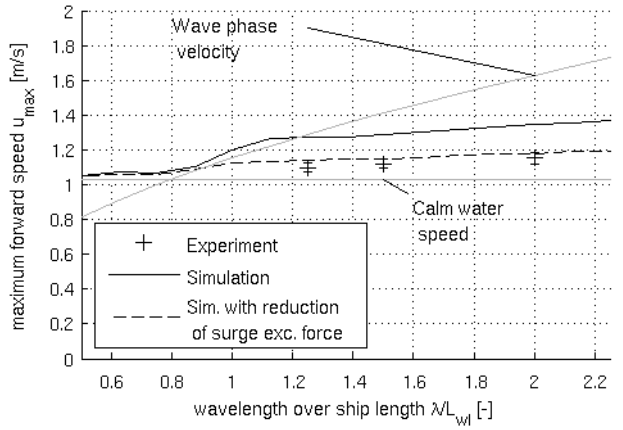


**FIGURE 14: Simulated and experimental maximum ship speed $u_{max}$ during straight line manoeuvres in following seas ($\beta = 0°$), with a wave steepness $H/\lambda = 1/25$ and different ratios of wavelength over ship length $\lambda/L_{wl}$.**

An error source in the simulations was the fact that the influence of the waves on the rudder and propulsion forces was neglected. The reduction of the rudder effectiveness due to the small relative velocity between the ship and the horizontal water velocity in the waves during surf-riding, which is often cited as one of the main reasons for broaching (Faltinsen [20]; Renilson [22]), was not modelled in the simulation model.

Turning circle manoeuvres at small frequency of encounter were performed with the *Lady Marianne* to study the ship behaviour in a seaway. Four different types of turning manoeuvres were performed, with different rudder angles $\delta_t$ and wave conditions, as shown in Tab. 3.

**TABLE 3: Waves and operational conditions during the turning circle manoeuvres at small frequencies of encounter. $\delta_t$=Rudder angle. RPM=propeller RPM, $\lambda/L_{wl}$= wavelength over ship length ratio. $H/\lambda$= wave steepness.**

| $\delta_t$ | RPM | $\lambda/L_{wl}$ | $H/\lambda$ |
|---|---|---|---|
| $-25°$ | 2750 | 1.50 | 1/25 |
| $-35°$ | 2750 | 1.50 | 1/25 |
| $-25°$ | 2750 | 2.00 | 1/25 |
| $-35°$ | 2750 | 2.00 | 1/25 |

The procedure used in the experiments and in the simulations was as follows:
(1) The ship is free, at rest, and positioned with $\psi = 0°$ between 2 and 2.5m from the wavemaker and between 1 and 1.5 m from the side of the tank.
(2) The wavemaker is activated at $t = -15\text{ s} - aT$, where $T$ is the wave period and $a = 15$ and 10 for $\lambda/L_{wl} = 1.50$ and 2.00, respectively.
(3) At $t = -15$ s, the propeller and the rudder autopilot are turned on. The propeller is controlled to rotate at the desired RPM, and the autopilot is controlling the rudder for the ship to navigate on a straight line in following seas.
(4) At $t = 0$ s, the turn is initiated by turning the rudder to the desired rudder angle $\delta_t$. The path of the ship during one of the experiments and the different steps in the procedure are shown in Fig. 15.

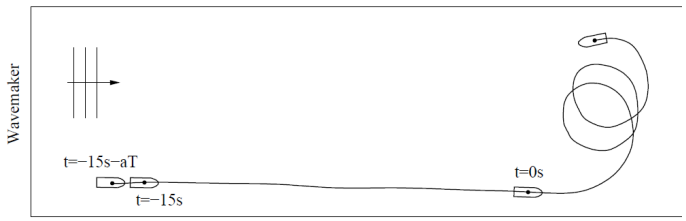


**FIGURE 15: Turning circle manoeuvre at small frequency of encounter. The ship is idle and free at $t = -15\text{ s} - aT$ when the wavemaker is activated. The propeller is activated at $t = -15$ s, and the turn is initiated at $t = 0$ s.**

For the simulations, the reduction coefficients mentioned in Eq. (10) were used. Although the reduction factors were only applicable for a forward speed $U = 1$m/s and in following seas, they were used for the complete simulations. The reduction coefficients induced a negative mean forward speed when the ship was freely drifting, but gave satisfactory results when the ship was moving forward. The comparison between simulated and experimentally recorded path of the ship during the turning circle manoeuvres is shown in Fig. 16. The line indicates the path of the ship for the same duration in time for the simulation and the experiment. The rudder starts to turn to $\delta_t$ when the ship is in $(X, Y) = (0,0)$.

The simulated turning circle manoeuvres were sensitive to the position of the ship on the wave when the turn was initiated. In the simulations, the time before the start of the turn was modified to enforce the same position on the wave as when the turn was initiated in the experiments.

The path of the ship in the turning circle manoeuvre was correctly simulated for the first half of the turn. The agreement between the simulated and experimental path was relatively poor for the rest of the turning motion, and the maximum distance between the simulated and experimental position of the ship at the end of the manoeuvres was $1.5L_{wl}$, where $L_{wl}$ is the ship length at the waterline. Possible reasons are that mean wave loads and the wave effect on rudder forces are neglected.

Zigzag manoeuvres at small frequency of encounter were performed in a way similar to the turning circle manoeuvres. The agreement between the simulated and the experimental path of the ship during the zigzag manoeuvres was good. In the zigzag manoeuvres, the path was very dependent on the balance between propulsion, wave and rudder forces, which were verified in the straight line manoeuvres in stern seas.

## 8 CONCLUSIONS

A new simulation model was developed and different kinds of experiments were performed to study the behaviour of a fishing vessel at small frequency of encounter in stern sea.

A simplified mathematical model was used for the simulations. The modules expressing the calm water resistance, the rudder forces, the propulsion forces, and the non-linear viscous forces, were expressed based on a mixture of theory, empiricism, and experimental results. By use of simple captive experiments, it was found that:

- the wake factor was varying with the ship forward speed,
- the cross-flow principle combined with the hull-lift forces simulates adequately the side forces on a ship, also for small drift angles ($|\beta| < 20°$)
- the slope of the rudder lift coefficient decreases with the rudder angle.

Free running manoeuvres in calm water were performed to validate the simulation model. Based on a sensitivity analysis during calm-water turning circle manoeuvres, it was found that the manoeuvring model is most sensitive to the rudder lift coefficient and the position of the flow separation section.

The wave-induced surge forces in following seas were measured by use of captive experiments in following seas. The simulated wave-induced surge forces over predicted the experimental results, probably because the interaction between the local steady and unsteady flow was not accounted for.

Free-running experiments at small frequency of encounter were performed and compared to simulations. Over-predicted wave-induced surge forces in following seas lead to simulations with surf-riding and broaching, which were not observed in the experiments.

Satisfactory agreement was obtained between the experimental and the simulated ship behaviour during manoeuvres at small frequency of encounter by reducing the wave excitation forces in surge, based on the results of the captive experiments in following seas.

## ACKNOWLEDGMENTS

This study was financially supported by the Norwegian Research Council, through the Centre for Ship and Ocean Structures (CeSOS) at the Norwegian University of Science and Technology (NTNU).

## REFERENCES

[1] de Kat, J. O. and Paulling, J. R. (1989), "The simulation of ship motion and capsizing in severe seas", *Transactions of the Society of Naval Architects and Marine Engineers*, vol. 97, pp. 139-168.

[2] Salvesen, N., Tuck, E. O. and Faltinsen, O. M. (1970), "Ship motions and sea loads", *Transactions of the Society of Naval Architects and Marine Engineers*", Vol. 78, pp. 250-287.

[3] Skejic, R., Faltinsen, O. M. (2008). "A unified seakeeping and maneuvering analysis of ships in regular waves", *Journal of marine science and technology*, Vol. 13, pp. 371-394.

[4] Ayaz, Z. (2003), Manoeuvring behaviour of ships in extreme astern seas, PhD thesis, Universities of Glasgow and Strathclyde, United Kingdom.

[5] Umeda, N., Hashimoto, H. and Matsuda, A. (2003), "Broaching prediction in the light of an enhanced mathematical model, with higher-order terms taken into account", *Journal of marine science and technology*, Vol. 7, pp. 145-155.

[6] Thys, M. (2013), Theoretical and experimental investigation of a free running fishing vessel at small frequency of encounter, PhD thesis, Norwegian university of science and technology, Trondheim, Norway.

[7] Beck, R. and Loken, A. (1989), "Three-dimensional effects in ship relative-motion problems", *Journal of ship research*, Vol. 33, pp. 261-268.

[8] Papanikolaou, A. and Schellin, T. (1992), "A three-dimensional panel method for motions and loads of ships with forward speed", *Ship technology research*, Vol. 39.

[9] McTaggart, K. (2002), Three dimensional ship hydrodynamic coefficients using the zero forward speed green function, Technical memorandum TM 2003-104, Defence R&D Canada.

[10] Cummins, W. E. (1962), The impulse response function and ship motions, Technical Report 1661, David Taylor Model Basin.

[11] Söding, H. (1982), "Prediction of ship steering capabilities", *Schiffstechnik*, Vol. 29, pp. 3-24.

[12] Digernes, T. (1982), An analytical approach to evaluating fishing vessel design and operation, PhD thesis, Norwegian university of science and technology.

[13] Ommani, B. (2013), Potential-flow prediction of a semi-displacement vessel including applications to calm-water broaching, PhD thesis, Norwegian university of science and technology, Trondheim, Norway.

[14] Oosterveld, M. W. C. (1970), Wake adapted ducted propellers, Technical Report 345, Netherlands Ship Model Basin.

[15] Journée, J. M. (1976), Prediction of speed and behaviour of a ship in a sea-way, Technical Report 427, Delft University of Technology, Ship Hydrodynamics Laboratory.
[16] Taylor, D. (1942), *The speed and power of ships: a manual of marine propulsion*, United States Government Printing Office
[17] Ankudinov, V., Kaplan, P. and Jacobsen, B. (1993), Assessment and principal structure of the modular mathematical model for ship maneuvrability prediction and real-time maneuvering simulations, *in* 'Proceedings of MARSIM'.
[18] Bertram, V: (2000), *Practical ship hydrodynamics*, Butterworth-Heinemann
[19] Inoue, S., Hirano, M., Kijima, K. and Takashina, J. (1981), "A practical calculation method of ship maneuvering motion", *International shipbuilding progress*, Vol. 28, pp. 207-222.
[20] Faltinsen, O. M. (2005), *Hydrodynamics of high-speed marine vehicles*, Cambridge university press.
[21] Söding, H. (1984), "Influence of course control on propulsion power", *Schiff und Hafen*, Vol. 36, pp. 63-68
[22] Renilson, M. (1982), An investigation into the factors affecting the likelihood of broaching-to in following seas, *in* 'Proceedings of the second international conference on stability of ships and ocean vehicles', pp. 551-564.

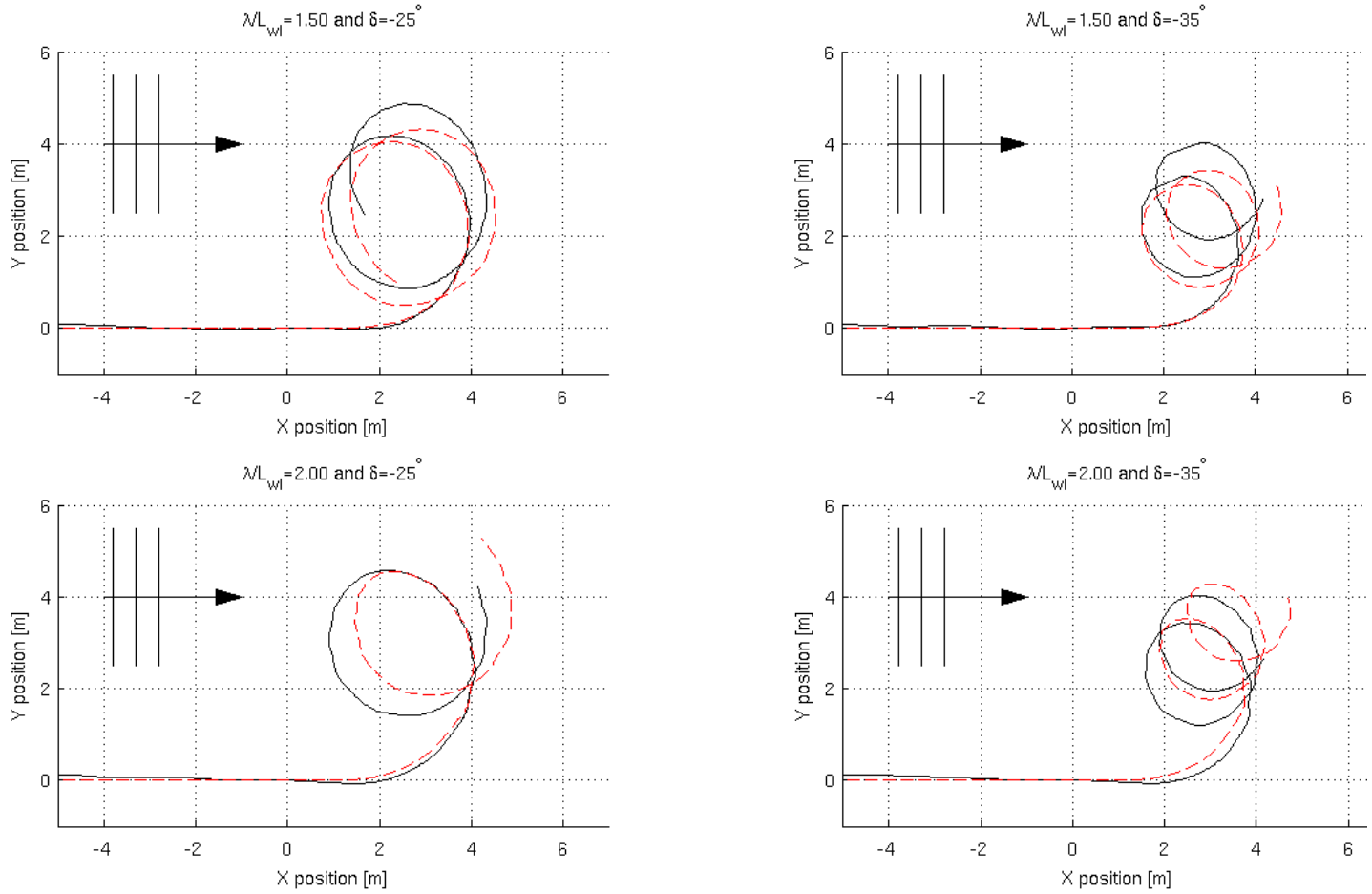


**FIGURE 16: Experimental (full line) and simulated path (dashed line) of the *Lady Marianne* during turning circle manoeuvres at small frequency of encounter. The wave steepness in the four manoeuvres is $H/\lambda = 1/25$. The turn is initiated when the ship is at the position (X,Y)=(0,0). $L_{wl}$ is the ship length at the waterline, and $\delta$ is the rudder angle during the turning motion. Propeller RPM of 2750, which corresponds to a calm water forward speed of 1.04 m/s ($Fn = 0.360$).**